Molecular Architecture Effect on Microphase Separation in Supramolecular Comb−Coil Complexes of Polystyrene-*block*-poly(2-vinylpyridine) with Dodecylbenzenesulfonic Acid: A_nB_n Heteroarm Star Copolymer

Bhanu Nandan,[†] Chia-Hua Lee,[‡] Hsin-Lung Chen,*[,†] and Wen-Chang Chen[‡,§]

Department of Chemical Engineering, National Tsing Hua University, Hsin-Chu 30013, Taiwan; Institute of Polymer Science and Engineering, National Taiwan University, Taipei 10617, Taiwan; and Department of Chemical Engineering, National Taiwan University, Taipei 10617, Taiwan

Received January 8, 2006; Revised Manuscript Received April 19, 2006

ABSTRACT: The microphase separation in a supramolecular comb−coil block copolymer formed by the stoichiometric complexation of an amphiphilic surfactant, dodecylbenzenesulfonic acid (DBSA), with the poly(2-vinylpyridine) (P2VP) blocks in a nonlinear heteroarm $(PS)_5(P2VP)_5$ star copolymer has been investigated. The hierarchical structure in the ordered state and the relevant order−disorder transitions (ODT) of the complex have been revealed using small-angle X-ray scattering (SAXS). The results were compared with those obtained previously for linear PS-*b*-P2VP(DBSA) and block-arm $(PS\text{-}b\text{-}P2VP)_5(PS)_5$(DBSA) complexes [*Macromolecules* **2005**, *38*, 10117] to illustrate the effect of block copolymer architecture on the self-assembly behavior of the supramolecular comb−coil complexes. The heteroarm $(PS)_5(P2VP)_5$(DBSA) complex exhibited structure-within-structure morphology in which the larger-scale PS cylindrical microdomains were embedded in the matrix consisting of the smaller-scale lamellar mesophase organized by the P2VP(DBSA) comb blocks. As observed previously for the linear PS-*b*-P2VP(DBSA) complex, the ODT temperature (T_{ODT}) of the copolymer domain in the heteroarm complex was appreciably higher than that of neat $(PS)_5(P2VP)_5$ due to the strong interblock repulsion caused by the increase in the polarity of P2VP blocks upon complexation with DBSA. Most interestingly, a significant increase in the T_{ODT} of the smaller-scale lamellar mesophase was observed in the heteroarm complex compared to that of its linear counterpart, and this was attributed to the lower entropy of transition due to the junction constraint. The interdomain distance of the copolymer domains in the heteroarm complex was smaller than that in the linear complex due to lower aggregation number of PS star arms in the cylindrical domains. However, the corresponding interdomain distance was significantly larger than that in the block-arm complex due to different type of intermolecular segregation occurring in the two kinds of star copolymers.

Introduction

It is well-known that block copolymers self-organize into a series of long-range ordered nanostructures due to repulsion between the covalently connected blocks.[1−7] Similar to block copolymers are polymers with comb-shaped architecture which also exhibit the propensity to self-organize in a similar way.[8] In comb-shaped polymers, the covalent or permanent bonding between the backbone and the repulsive side chains may be replaced by the physical bonding such as ionic bonds, hydrogen bonds, and metal-mediated coordination bonds to form supramolecules which may analogically self-organize to form mesomorphic nanostructures.[9−21] In a special case, if one of the blocks of a diblock copolymer is selectively complexed with amphiphilic molecules, the resulting supramolecular comb−coil diblock may exhibit hierarchical assembly at two length scales,[19] namely, a larger-length-scale assembly due to the microphase separation between the comb and coil blocks and another shorter-length-scale ordering inside the comb block domains driven by the microphase separation between the backbone and the side chains. Such supramolecular comb−coil complexes have been drawing significant interest recently due to their potential use as functional materials in electrical, optical, and other functionalities.[22−34] The self-organized domains at multiple length scales offer switchlike controls of material functionalities by the relevant order−disorder or order−order transitions.[13]

The self-assembly behavior of the supramolecular comb−coil complexes formed by the linear diblock copolymers is more or less well understood. Recently, we have been interested in exploring the microphase separation behavior in the supramolecular comb−coil complexes where the block copolymer backbone has a nonlinear architecture.[35] The novel macromolecular architectures in nonlinear block copolymers offer a promising way to modulate the free energy balance and thus the phase state of the block copolymers.[36−39] Like linear diblock copolymers, these polymeric species undergo microphase separation to form well-ordered structures. Hence, the different architecture results naturally in much slower phase separation kinetics and modification of the phase behavior.[4,7,40−50] Thus, the block copolymer molecular architecture may also considerably influence the phase state of the supramolecular comb−coil complexes.

In a previous study, we investigated the molecular architecture effect on the microphase separation in the supramolecular comb−coil complexes using a $(AB)_n(A)_n$-type block-arm polystyrene-*block*-poly(2-vinylpyridine) (PS-*b*-P2VP) with the P2VP block complexed with an amphiphilic surfactant, dodecylbenzenesulfonic acid (DBSA).[35] Some remarkable differences in the phase transition temperatures and interdomain spacing

[†] National Tsing Hua University.
[‡] Institute of Polymer Science and Engineering, National Taiwan University.
[§] Department of Chemical Engineering, National Taiwan University.
* To whom correspondence should be addressed.

10.1021/ma060042t CCC: $33.50
Published on Web 05/25/2006

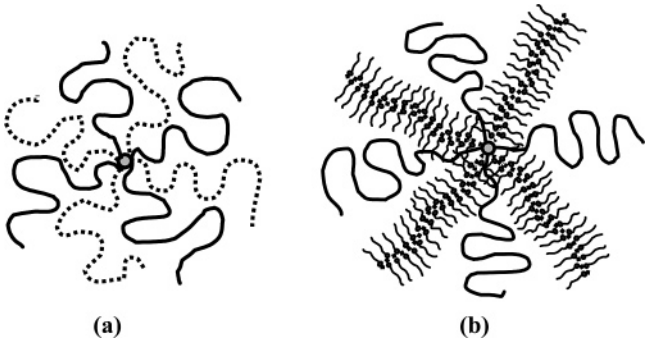

Figure 1. Schematic representation of the molecular architecture of (a) $(PS)_5(P2VP)_5$ heteroarm star diblock copolymer and (b) $(PS)_5$-$(P2VP)_5$ heteroarm star diblock copolymer complexed with a surfactant. The solid lines represent PS blocks, and the dashed lines represent P2VP blocks. The surfactant was selectively bound to P2VP bock. The actual number of arms in the star copolymer used in this study is more than that shown in the figure.

between the block-arm complex and its linear counterpart were observed. In the present study, we direct our attention to the comb−coil complexes formed by a A_nB_n heteroarm star copolymer. As shown in Figure 1a, heteroarm star copolymers are star-shaped molecules constituted of a central core bearing arms of pure polymer A and pure polymer B. The previous studies have shown that, due to the chain crowding at the star junction, the phase behavior and the domain spacing of neat A_nB_n heteroarm star copolymers differ considerably from those of the linear AB diblock copolymers.[36,38−40,44,46−50]

The system under study is the complex of PS_5P2VP_5 heteroarm star copolymer with DBSA. Our approach here is similar to that described in our previous work.[35] First, we study the self-assembly of the neat PS_5P2VP_5 heteroarm star copolymer. The molecular architecture effect on the microphase separation behavior in neat PS_5P2VP_5 will be compared with that of neat PS-*b*-P2VP and block-arm $(PS\text{-}b\text{-}P2VP)_5(PS)_5$ copolymer discussed in our previous work. Then we proceed to study the microphase separation in the complex of PS_5P2VP_5 with DBSA. We will show that hierarchical structures with two distinct length scales were formed despite the architectural complexity of the copolymer. Furthermore, the phase transition behavior and the interdomain distance in the complex will be compared with that reported in our previous work for linear PS-*b*-P2VP(DBSA) and block-arm $(PS\text{-}b\text{-}P2VP)_5(PS)_5$(DBSA) comb−coil complexes.

Experimental Section

Synthesis and Characterization of Neat Block Copolymers. The A_nB_n type of PS−P2VP heteroarm star copolymer was synthesized by the sequential anionic living polymerization similar to the P2VP-*block*-poly(*tert*-butyl acrylate) heteroarm star copolymer reported in the literature,[51] as shown in Scheme 1. First some living PS arms were synthesized using *sec*-butyllithium as the initiator. The reaction temperature was maintained at −78 °C. These PS arms were then joined together in the second step by reacting the living PS chains with a small amount of divinylbenzene (DVB). A star-shaped $(PS)_n$ was thus formed, bearing a number of active sites at the DVB core which was equal to the number of the attached PS arms. In the third step, a second generation of P2VP arms grew from the cores on adding 2-vinylpyridine (2VP) to the reaction mixture. The living anionic polymerization was terminated by methanol, precipitated in hexane, and then filtered out to obtain the polymer product. The product was subsequently purified by extraction using cyclohexane−heptane (v/v, 95/5) followed by fractionation by GPC to remove the unattached PS arms present due to accidental deactivation during the DVB polymerization. The presence of a single sharp peak in the GPC curve of the purified

Scheme 1

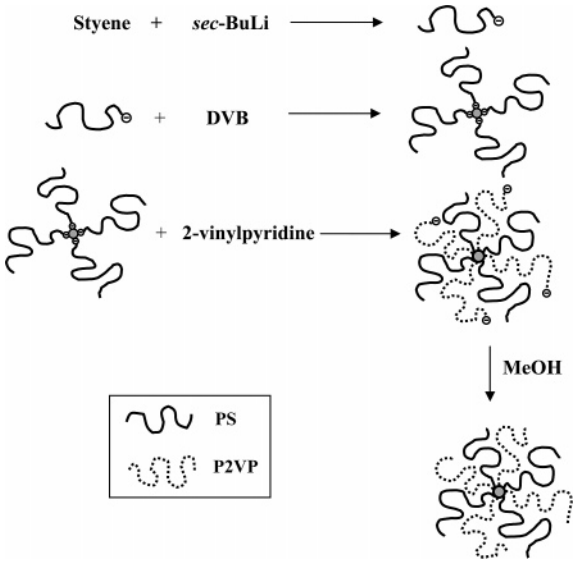

sample (cf. Supporting Information) indicated that a heteroarm copolymer with fairly uniform arm number and controlled molecular weight was obtained after the purification. However, it should be noted that the standard separation techniques such as fractionation did not necessarily result in product with monodisperse arm number for star copolymers.[50,52] It has also been shown that the conventional polymer characterization techniques including GPC were insufficient to establish the purity of the copolymers with complex architecture.[50,52] Hence, we must indicate here that a slight polydispersity in arm number could exist in our sample due to the random character of polymerization of DVB forming the core of the copolymer, such that the functionality of the copolymer given here corresponded to a mean value. According to Zhu et al.,[50] most of the results reported in the literature regarding heteroarm stars were derived from the polymers produced by similar synthetic routes, and thus these materials most likely had similar polydispersity in arm number. Nevertheless, because the peculiar phase behavior reported here was governed by the junction constraint associated with the star architecture and no quantitative analysis using arm number as a parameter was attempted, the polydispersity in arm number would not have any significant effect on the issues discussed in this work as long as the copolymer under study possessed the heteroarm architecture.

The copolymer obtained after the purification had a M_w of 51 870 with a polydispersity index of 1.1, and the volume fractions of PS in the neat copolymer and the stoichiometric complex were 0.50 and 0.20, respectively. The average number of arms in the heteroarm star copolymer was 9.0; therefore, the copolymer was denoted as PS_5P2VP_5 and henceforth will be referred as HA. The detailed molecular characteristics of HA along with that of the linear diblock (LA) and the block-arm (BA) copolymers investigated in our previous work are given in Table 1.

Complex Preparation. The HA star copolymer and DBSA were first dissolved in THF separately to form clear solutions. The HA-(DBSA) complex with binding fraction $x = 1.0$ was then prepared by combining appropriate quantity of the two solutions. The binding fraction represented the average number of DBSA molecules bound with a P2VP monomer unit. The solution was stirred for 24 h followed by slowly evaporating the solvent at room temperature. The samples were finally dried in a vacuum at 60 °C for 2 days to remove the residual solvent.

SAXS Measurements. SAXS measurements were performed using a Bruker Nanostar SAXS instrument. The X-ray source, a 1.5 kW X-ray generator (Kristalloflex 760) equipped with a Cu tube, was operated at 35 mA and 40 kV. The scattering intensity was detected by a two-dimensional position-sensitive detector (Bruker AXS) with 512 × 512 channels. The area scattering pattern has been radially averaged to increase the photon counting

Table 1. Molecular Characteristics of Polystyrene/Poly(2-vinylpyridine) Copolymers

sample[a]	M_w[b] overall	M_w[c] PS-arm	M_w[d] PS-arm	M_w[e] P2VP-arm	M_w/M_n	N[f]	f_{PS}[g]	f_{PS}[h]
HA	51 870	5750		5740	1.1	9.0	0.50	0.20
BA	55 950	1150	3480	6760	1.3	4.9	0.41	0.14
LA	8 790	4480		4310	1.1		0.51	0.20

[a] "HA", "BA", and "LA" represent heteroarm, block-arm, and linear diblock copolymers, respectively. [b] Weight-average molecular weight of the whole macromolecule. [c] Weight-average molecular weight of PS block in a single diblock arm. [d] Weight-average molecular weight of a free PS arm in the block-arm star copolymer. The number of such arms in one macromolecule is the same as the number of diblock arms. [e] Weight-average molecular weight of P2VP block in a single diblock arm. [f] Average functionality, i.e., average number of PS-*b*-P2VP arms in the star copolymer. [g] Overall volume fraction of PS in the neat copolymer. [h] Overall volume fraction of PS in the copolymers after complexation with DBSA.

efficiency compared with the one-dimensional linear detector. The intensity profile was output as the plot of the scattering intensity (I) vs the scattering vector, $q = 4\pi/\lambda \sin(\theta/2)$ (θ = scattering angle). All scattering data were corrected by the empty beam scattering, the sensitivity of each pixel of the area detector, and thermal diffuse scattering. Details regarding correction for thermal diffusion scattering have been described elsewhere.[35] Temperature-dependent SAXS measurements were performed under vacuum to minimize the thermal degradation of the sample. The sample was first equilibrated at the measuring temperature for 20 min followed by 1 h data acquisition.

Results and Discussion

Self-Assembly and ODT of the Neat Heteroarm Star Copolymer. For the convenience of presentation, the PS_5P2VP_5 heteroarm star copolymer is denoted by "HA". Figure 2a,b shows the temperature-dependent SAXS profiles of neat HA in the temperature range 25−290 °C. The SAXS profiles at low temperatures showed a relatively sharp primary maximum at 0.45 nm^{-1} and a weak second-order peak near 0.90 nm^{-1}, indicating the formation of a lamellar morphology consisting of alternating PS and P2VP lamellae. This morphological structure was expected considering the composition of the HA copolymer (i.e., the volume fraction of PS, $f_{PS} \approx 0.50$). The interlamellar distance at 25 °C calculated from Bragg's equation ($D = 2\pi/q_m$ with q_m being the position of the primary diffraction peak) was 14.0 nm. As the temperature increased, the higher-order peak gradually diminished, and the intensity of the primary peak decreased along with a peak broadening. A sharp and remarkable change in the scattering pattern was discernible at 180 °C due to the occurrence of ODT. The broad peak observed in the disordered state (T > 180 °C) was attributed to the "correlation-hole" effect, which reflected the concentration fluctuations of the copolymer segments in the disordered state.[1,53]

The abrupt change of the scattering pattern across the ODT enabled the determination of T_{ODT} using the plots of (i) the reciprocal of the maximum scattering intensity (I_m^{-1}) vs the reciprocal of the absolute temperature (T^{-1}) and (ii) D vs T^{-1}. A discontinuous change in these plots at a particular temperature indicates the occurrence of ODT. Figure 3 presents the plots of I_m^{-1} and D vs T^{-1} for the HA copolymer. A significant drop in the intensity was observed on heating to 180 °C, which showed that T_{ODT} of neat copolymer located near this temperature. Moreover, the plot of D vs T^{-1} also showed a sharp decrease as the temperature was raised to 180 °C.

In our previous article we had shown that T_{ODT} of a linear PS-*b*-P2VP diblock copolymer, whose block molecular weights and composition were equivalent to those of the present HA copolymer, located at about 150 °C.[35] Hence, the T_{ODT} of the HA copolymer was about 30 °C higher than that of the linear diblock. Olvera de la Cruz and Sanchez[36] were the first to predict the position of ODT for A_nB_n copolymer (assuming equal segmental lengths and volumes for A and B monomers) using a mean-field theory. They found that for symmetric A_nB_n, with

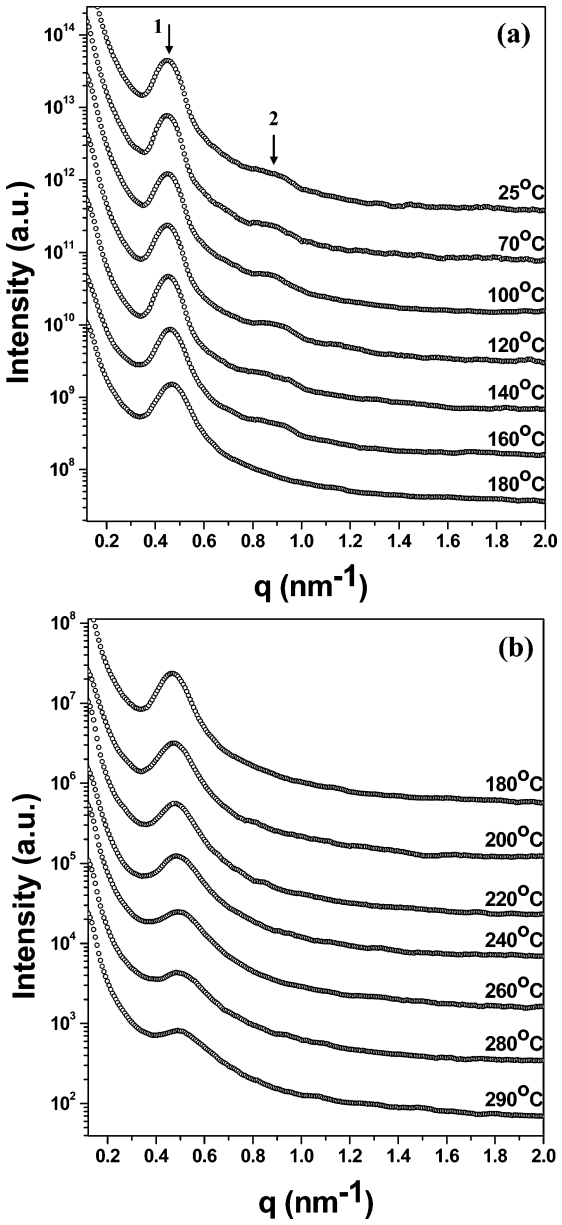

Figure 2. Temperature-dependent SAXS intensity profiles of neat HA diblock copolymer collected in-situ from (a) 25 to 180 °C and (b) 180 to 290 °C in a heating cycle.

each A and B arm consisting of $N/2$ monomers, the ODT occurs at

$$(\chi N)_{ODT} = 10.495 \qquad (1)$$

for all values of n (where χ is the Flory interaction parameter). This means that the T_{ODT} should be identical for all symmetric A_nB_n irrespective of n. However, it had been shown recently that,[44] in contrast to the mean-field prediction, the T_{ODT} of

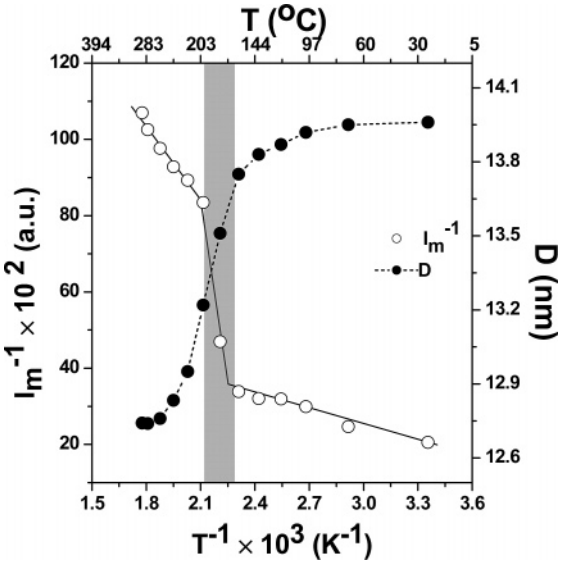

Figure 3. I_m^{-1} and D vs T^{-1} plot of neat HA diblock copolymer for T_{ODT} determination.

symmetric A_nB_n heteroarm star copolymer was always higher than that of the corresponding AB linear diblock, as was also observed in the present study. The composition fluctuations, which were not considered in the mean-field theory, became important for the symmetric block copolymers near ODT.[44,54] After a standard fluctuation correction, the ODT of the symmetric diblock was found to occur at a higher value of χN (or a lower T_{ODT}) than that predicted by the mean-field theory.[54] A possible cause for the observed difference in T_{ODT} between A_nB_n ($n \geq 2$) and linear AB diblock was the different strength of composition fluctuations due to difference in molecular architecture. However, although the standard fluctuation correction did predicted a difference in T_{ODT}, it was still insufficient to account for the experimental results.[44] Recently, Buzza et al.[44] suggested that the large increase in T_{ODT} arose from a combination of composition fluctuations and different degrees of non-Gaussian stretching in the two systems at or near T_{ODT}. The higher degree of chain stretching also led to a larger interlamellar spacing in the heteroarm star copolymers compared to that in the linear counterpart. The stretching of the polymer chains was most likely due to dissimilar interactions between clusters of like monomers, though other mechanisms such as chain stiffening and crowding effects near star branch point were not precluded. Buzza et al.[44] showed that the difference in T_{ODT} observed in their system was consistent with the degree of chain stretching observed experimentally. However, in the present study we found that although the T_{ODT} of HA was greater than that of LA, the interlamellar distance of these two systems was close.

It was rather unexpected that the domain spacings of HA and LA were similar as the previous studies had predominantly shown that interlamellar distance was larger in the heteroarm star copolymers compared to the linear copolymers of equivalent block length.[44,46,48−50] Grayer et al.[48] studied PS_6P2VP_6 heteroarm copolymer and found that the dependence of the interlamellar distance on block length deviated from the $N^{2/3}$ scaling law (known for linear diblocks). In this case, the interlamellar distance followed N^{μ} scaling law with $\mu > 2/3$. Nevertheless, the architecture effect on the domain spacing was most significant in the region of intermediate arm length (with $N \sim 400-500$) and diminished at higher N when the arms became sufficiently long to screen the effect of conformational

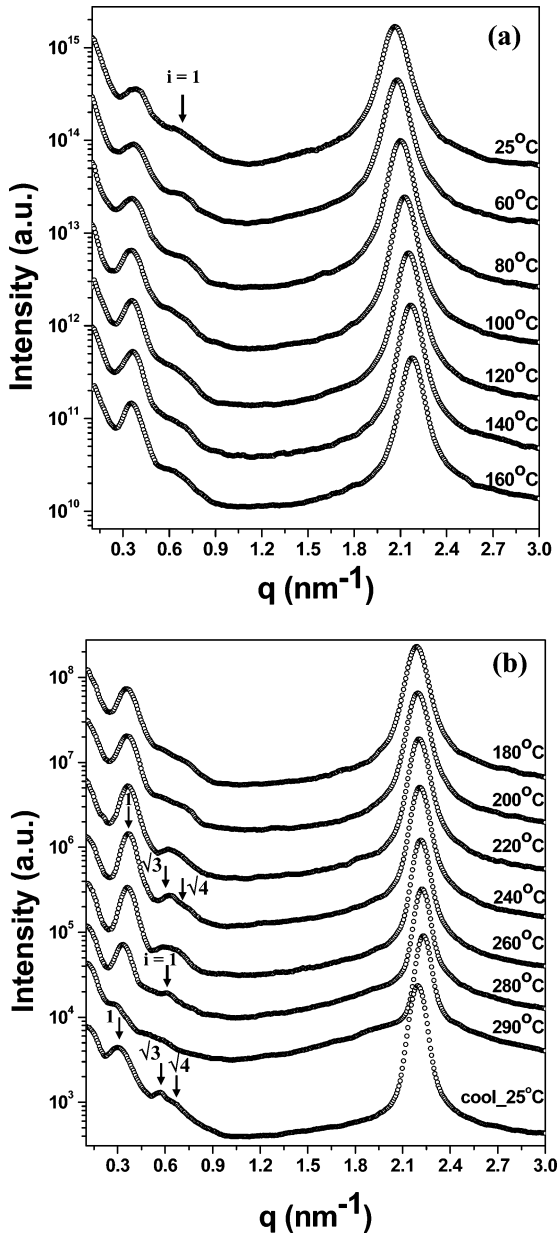

Figure 4. Temperature-dependent SAXS intensity profiles of HA(DBSA) comb−coil complex collected in-situ from (a) 25 to 160 °C and (b) 180 to 290 °C in a heating cycle. The SAXS profile obtained after cooling the sample from 290 to 25 °C is also included in (b).

peculiarities at the interface. The similar interdomain distance between HA and LA studied here might be due to the relatively low molecular weight of the system ($N \sim 70-80$) because the ratio $D_{HA}/D_{LA} \sim N^{(\mu-2/3)}$ decreases with decreasing N; namely, the difference in the interlamellar distance between heteroarm and linear block copolymers is expected to become more insignificant at smaller N.

Hierarchical Structures and ODT of the Comb−Coil Complexes. The phase behavior of the HA(DBSA) supramolecular comb−coil complex was probed by SAXS. Figure 4a,b displays the temperature-dependent SAXS profiles of the HA(DBSA) complex. The SAXS profile at 25 °C showed a scattering maximum at $q = 0.38$ nm^{-1} and a broad shoulder (marked by "$i = 1$") at $q \cong 0.69$ nm^{-1}. Another peak of strong intensity was observed in the high-q region at $q = 2.07$ nm^{-1}. The SAXS peaks in the low-q region were associated with the larger-scale structure due to microphase separation between PS and P2VP(DBSA) blocks (giving rise to copolymer domains).

On increasing the temperature the two low-q peaks became more intense. At 240 °C the higher-order scattering peaks associated with the long-range order of the copolymer domains became visible (Figure 4b). The lattice scattering was even clearer in the SAXS profile of the 240 °C-annealed sample collected using synchrotron radiation source (see Supporting Information). The positions of the lattice peaks here closely followed the ratio of $1:3^{1/2}:4^{1/2}$, indicating that the complex contained hexagonally packed PS cylinders in the P2VP(DBSA) matrix. The cylinder morphology was also confirmed by TEM for the as-cast complex (see Supporting Information). Hence, the copolymer domain morphology of HA(DBSA) complex was similar to that observed for LA(DBSA) complex reported in our previous work.[35]

The long-range order of the PS cylinders was not attained in the as-cast state since the corresponding SAXS profile only showed a broad scattering peak at 0.38 nm^{-1} (corresponding to the interdomain distance of 16.5 nm^{-1}) (cf. Figure 4a). The shoulder marked by "$i = 1$" was attributed to the first-order form factor maximum ($q_m^{i=1}$). The average radius of the PS cylinders deduced from the form factor peak position via $R = 4.98/q_m^{i=1}$ was 7.2 nm. As will be discussed in more detail later, the interdomain distance and the cylinder radius in HA(DBSA) complex were smaller than those in the LA(DBSA) complex but larger than those in the BA(DBSA) complex. The positional order of PS cylinders was enhanced on heating, and the equilibrium hexagonal lattice was attained near 240 °C. On heating to 260 °C, the higher-order lattice peaks diminished, showing that the grain size of the hexagonally packed PS cylinders became smaller at this temperature due to thermal agitation. As the temperature was further increased to 280 °C, the intensity of the primary scattering peak decreased appreciably. This large intensity drop was also demonstrated from the I_m^{-1} vs T^{-1} plot in Figure 5a, where an abrupt change of I_m^{-1} was clearly discerned between 260 and 280 °C. Since the form factor peak still persisted at 280 °C, the large drop in intensity was not associated with the ODT that transformed the system into a homogeneous melt. The intensity drop may alternatively be attributed to the occurrence of a thermal fluctuation-driven lattice disordering of the PS domains. In other words, PS cylinders exhibited short-range liquidlike order at 280 °C.

It should be noted that the peak broadening and the intensity drop observed at elevated temperatures were not primarily caused by thermal degradation. As can be seen in Figure 4b, the SAXS profile obtained after cooling the sample from 290 to 25 °C indicated that the equilibrium hexagonally packed cylinder morphology was recovered. This thermal reversibility showed that the sample was reasonably thermally stable even at the highest temperature accessed in the SAXS experiment, and the morphological transformation from hexagonally packed cylinders to disordered cylinders upon heating was real. The insignificant effect of thermal degradation on the phase transition behavior of the complex was corroborated by the increase of the intensity of the high-q peak corresponding to small-scale structure in the complex (to be discussed latter) on cooling from 290 to 25 °C and also by the thermal reversibility of the birefringent pattern associated with smaller-scale lamellar mesophase observed in the temperature-dependent polarized optical microscopy (POM) experiment (cf. Supporting Information).

Hashimoto et al.[55−58] have done extensive studies on the phase transitions of neat block copolymers and their blends with homopolymers, where the system with spatially ordered microdomains attained a disordered micelle structure before entering a micelle-free homogeneous state. According to these studies when a highly asymmetric block copolymer containing bcc-packed spheres was heated, it first underwent a lattice disordering transition (LDT) at a temperature denoted by T_{LDT}, giving rise to a disordered arrangement of spheres at thermal equilibrium. At further higher temperature a demicellization transition (DMT) occurred at T_{DMT} where the micelles disappeared and the system transformed into the micelle-free homogeneous state. However, for symmetric or nearly symmetric diblock copolymers forming lamellae or cylindrical microdomains, LDOT and DMT essentially degenerated into a single transition. In this case, the long-range ordered microdomains transformed directly into the homogeneous phase at T_{ODT}. Two factors basically distinguished the two different situations described above: (i) the thermodynamic stability of the domain and (ii) the thermodynamic stability of the lattice. In sphere-forming systems, domain stability overwhelmed the lattice stability; the lattice was thus more susceptible to the

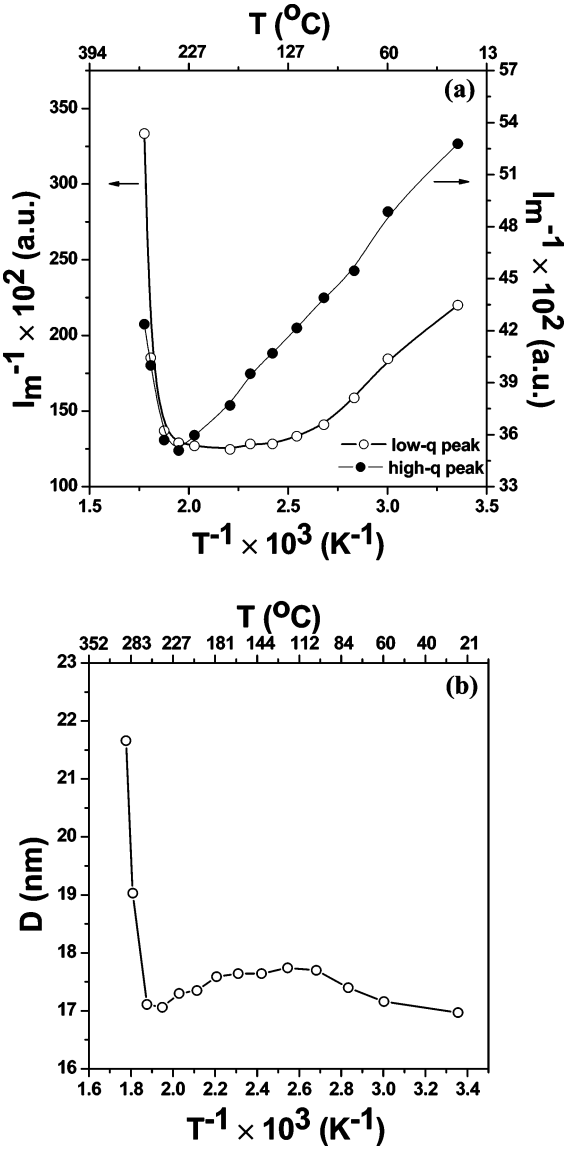

Figure 5. (a) I_m^{-1} vs T^{-1} plots for estimating the phase transitions of the larger-scale structure formed by copolymer domains and the smaller-scale structure formed by P2VP(DBSA) comb blocks in HA(DBSA) complex. (b) D vs T^{-1} plot for HA(DBSA) complex. D corresponds to Bragg's spacing and the most probable spacing of large-scale structure formed by the copolymer domains in the ordered and disordered state, respectively.

thermal agitation than the domain, such that the lattice disintegrated at a lower temperature than the micelles. However, in lamellae-forming or cylinder-forming systems, the two factors were nearly equally important. Thus, domains and lattices were destroyed at nearly the same temperature.

However, the hexagonally packed PS cylinders in the present HA(DBSA) complex did undergo a lattice disordering at 280 °C. In this case, the PS domains were highly stable because the strong repulsion between the polar P2VP(DBSA) blocks and the nonpolar PS blocks prevented the mixing of the two types of block chains. On the other hand, the lattice stability might not be as strong, since the P2VP(DBSA) matrix was fluidlike and the intense thermal fluctuations in this phase may perturb the ordered packing of the PS domains.

The micelle-free homogeneous state was not accessible for the HA(DBSA) complex within the experimental temperature range, showing that its T_{ODT} was higher than 290 °C. Hence, the T_{ODT} of the HA copolymer was raised by more than 100 °C upon complexation with DBSA. A similar increase of T_{ODT} was also found for the LA(DBSA) complex in our previous study[35] and was attributed to the increased polarity of P2VP blocks on complexation with DBSA because of the presence of an ionic moiety.

Figure 5b displays the interdomain distance as a function of T^{-1}. A discontinuous change in D was observed at 260 °C, which corresponded to a transition from the hexagonal lattice to the disordered PS cylinder structure. D in the disordered cylinder phase was found to be larger than that in the ordered state. Kim et al. had made a similar observation in a sphere-forming polystyrene-*block*-poly(ethylene-*co*-but-1-ene)-*block*-polystyrene (SEBS-8) triblock copolymer.[59] According to them, the smaller D and the smaller radius of the spheres in the bcc lattice compared with those in the disordered micelle state resulted from the constraint of the bcc lattice; namely, the spheres in a regular bcc phase were slightly collapsed compare with those in the disordered state. This was also reported for a polystyrene-*block*-polyisoprene-*block*-polystyrene (SIS) copolymer by Sakamoto et al.,[60] who attributed this increase in D upon the LDT to the broken symmetry. However, the increase of D across the LDT in the present HA(DBSA) complex was very significant, so some other factors which are not clear at present may also be responsible for the observed behavior.

We now turn to the temperature dependence of the high-q scattering peak located at 2.07 nm^{-1}. This peak was attributed to the primary diffraction maximum from the smaller-scale lamellar structure (with an interlamellar distance of 3.0 nm) organized by the P2VP(DBSA) comb blocks.[35] The presence of the lamellar mesophase was also supported by the POM observation showing the mesomorphic birefringent pattern (see Supporting Information). Hence, the HA(DBSA) comb−coil complex self-organized into a cylinder-within-lamellae morphology. The morphology of HA copolymer before and after complexation with DBSA is schematically illustrated in Figure 6a,b.

As evidenced from Figures 4b and 5a, the P2VP(DBSA) lamellar peak remained intense almost up to 260 °C. The intensity of this peak decreased when the sample was heated to 280 °C, where the scattering peak superposed on a broad halo. This indicated disordering of some lamellar domains due to dissociation of hydrogen-bonded DBSA from the P2VP blocks.[35] However, a significant portion of the lamellar domains retained at the highest accessible temperature (i.e., 290 °C) in the present study.

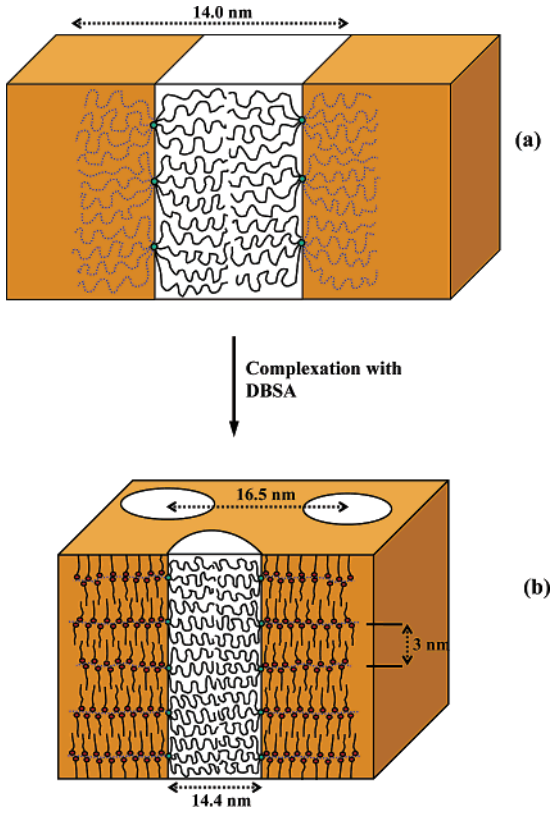

Figure 6. Schematic illustrations of the (a) lamellar morphology formed in neat HA copolymer and (b) hierarchical structure formed in HA(DBSA) complex where cylindrical microdomains of PS are embedded in the lamellar mesophase formed by P2VP(DBSA) comb blocks.

In the case of LA(DBSA) complex the ODT of the P2VP(DBSA) lamellar domains occurred near 220 °C;[35] however, the stability of the lamellar mesophase increased significantly in the HA(DBSA) complex as it remained stable up to almost 280 °C. It is noted that the binding mode of DBSA to P2VP in both complexes was the same; hence, the observed behavior must be due to the different architecture of the constituting copolymers. Let us understand why it is so by looking at the morphological changes across the ODT, as illustrated in Figure 7 for a simple linear comb−coil complex. At lower temperatures the complex shows hierarchical self-assembly where the domains formed by the coil blocks pack in the matrix composing of the smaller-scale ordered structure formed by the comb blocks (I). In this case, the backbone attached with the surfactant molecules may have to stretch significantly to allow the densely grafted surfactant molecules to pack to form a lamellar structure. When the complex is heated to a particular temperature, the smaller-scale structure is disrupted, and furthermore the weakly bonded surfactants dissociate from the comb blocks (II). The surfactant molecules in this case act like a selective solvent for one of the blocks, and the originally highly stretched chains in (I) can now relax, leading to an increase of the interfacial area of the copolymer domain formed by the coil blocks. Finally, at further higher temperatures, the surfactant becomes a nonselective solvent and diffuses into the other domain, transforming the system into a homogeneous melt (III). The HA(DBSA) complex is expected to exhibit a similar sequence of phase transition.

Considering the transition from I to II as a first-order transition, then the T_{ODT} of the smaller-scale lamellar mesophase is given by $T_{ODT} = \Delta H_t/\Delta S_t$, with ΔH_t and ΔS_t being the enthalpy and entropy of transition, respectively. Since the

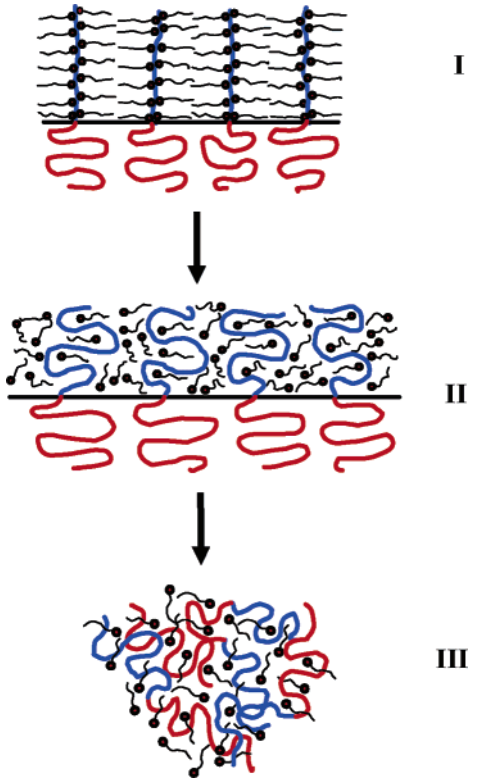

Figure 7. Schematic illustration of the morphological transitions which occur when a hierarchically organized supramolecular comb−coil complex is heated. (I) At lower temperature the complex exhibits microphase-separated structure at two distinct length scales. (II) As the complex is heated to a particular temperature, the smaller-scale structure formed by the comb blocks is disrupted. The interfacial area of the larger-scale copolymer domain increases here because the coronal block chains originally bound with the surfactant molecules can relax now. (III) At further higher temperatures, the surfactant becomes a nonselective solvent which makes the whole system homogeneous.

enthalpic term is almost same for both LA(DBSA) and HA(DBSA) complexes, the difference in T_{ODT} should stem from the difference in the transition entropy. This could be explained using the theoretical treatment given by Olvera de la Cruz and Sanchez for explaining the difference in ODT between neat LA and HA copolymers.[36] The entropy of HA(DBSA) complex is lower than that of LA(DBSA) complex in I because of the additional constraints on the PS−P2VP junction point at the interface; i.e., forming an PS_nP2VP_n star from nPS_1P2VP_1 diblocks is entropically unfavorable. The structure in II is also affected by this junction constraint, and hence the HA(DBSA) complex in II also has a lower entropy than the LA(DBSA) complex. Let us assume that joining two diblock chains from 2AB to A_2B_2 together reduces the entropy in I by $k_B \ln V_I$ and II by $k_B \ln V_{II}$, with V_I and V_{II} being the volume of the interfacial region formed by the microphase separation between the two blocks in the two states. Since disordering of the smaller-scale structure from I to II increases the area of the interface, $V_I < V_{II}$. If ΔS_0 is the transition entropy per diblock chain in a linear diblock complex, the transition entropy (per AB block chain) in the A_nB_n complex to a first approximation would be

$$\Delta S_t = \Delta S_0 - \left[\frac{n-1}{n}\right] \ln\left(\frac{V_{II}}{V_I}\right) \qquad (2)$$

The $1/n$ factor arose because the formation of an A_nB_n star from nA_1B_1 reduces the number of copolymer molecules in the system by a factor of $1/n$. Hence, the entropy of transition was lower

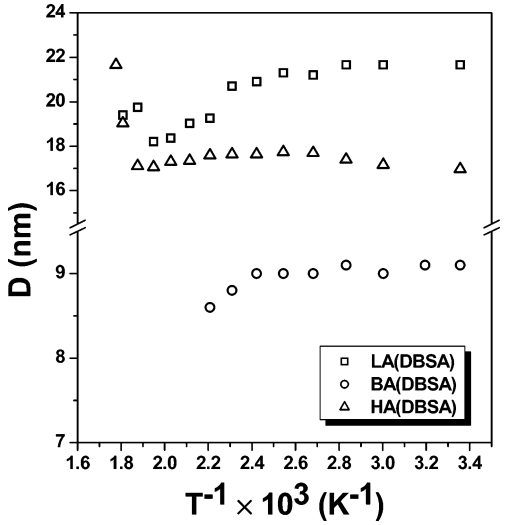

Figure 8. Comparative D vs T^{-1} plots of HA(DBSA), LA(DBSA), and BA(DBSA) complex, where D is the interdomain distance corresponding to larger-scale copolymer domain structure.

in HA(DBSA) complex according to eq 2, which then caused an increase of T_{ODT} for the smaller-scale lamellar mesophase.

Finally, it would be worthwhile to consider the effect of molecular architecture on the copolymer domain spacing in the comb−coil complexes. Figure 8 shows a comparative plot of the interdomain distance of the large-scale copolymer domains as a function of T^{-1} for LA(DBSA), BA(DBSA), and HA(DBSA) complexes. D in the HA(DBSA) complex was observed to be smaller than that in the LA(DBSA) complex, but it was significantly larger than that in the BA(DBSA) complex. The small interdomain distance in the HA(DBSA) complex compared to LA(DBSA) was attributed to the lower aggregation number of the PS blocks within the cylindrical microdomains due to its particular architecture. It had been reported that heteroarm star copolymers formed micelles with lower aggregation number in a selective solvent,[61,62] which might be due to better saturation of the core−corona interface by the fewer corona chains. Because of localization of the junction points at the interface, the volume available to each arm was less than the simple linear diblock.

The difference in the interdomain distance between the HA(DBSA) and BA(DBSA) complex was more striking since both complexes have starlike structure. This interesting behavior may be explained by considering the recent Monte Carlo simulation results obtained by Chang et al.[63] for explaining the self-assembly of star copolymers in selective solvents. According to the simulation results for the spherical micelles, the block-arm star copolymers tended to form unimolecular micelle structure since the copolymer molecules always showed intermolecular repulsions, which made them rather difficult to form multimolecular micelles. By contrast, the heteroarm star copolymer displayed Janus segregation, leading to intermolecular attraction and hence the formation of multimolecular micelles. Therefore, the aggregation number (per unit length of the cylinder) of the PS blocks in the cylindrical microdomain of HA(DBSA) complex was much higher than that in BA(DBSA), as shown in Figure 9, thereby leading to a larger PS domain size in the former. Furthermore, it can be easily shown that, under a given cylinder volume fraction, the larger cylindrical domain will result in a larger thickness of the corona surrounding the microdomain. Hence, the coronal thickness in the BA(DBSA) complex was also smaller than that in the HA(DBSA) complex. As shown in Figure 9a and discussed in detail in our

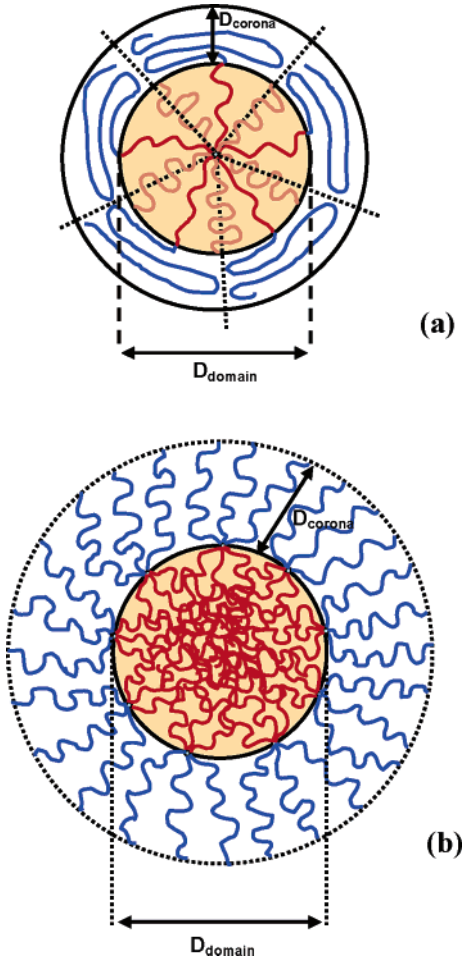

Figure 9. Schematic illustration of chain conformation in the microphase-separated structures of the (a) BA(DBSA) complex and (b) HA(DBSA) complex. The figure shows the cross-sectional view of cylindrical microdomains with DBSA molecules (not shown in the figure) aligning normal to the paper plane.

previous work,[35] the BA copolymer used in our study consisted of several free PS chains apart from the PS-*b*-P2VP diblocks junctioned to a common core. The presence of these free PS chains in the cylindrical microdomains increased the interfacial area available for the P2VP coronal chains. Hence, the P2VP chains had to fold in the direction perpendicular to the interface for efficient space filling, and this would result in a smaller corona thickness. Consequently, the smaller microdomain size and the thinner corona in BA(DBSA) complex due to the peculiar architecture of BA used in our study gave rise to the large difference in interdomain distance between HA(DBSA) and BA(DBSA) complexes.

Conclusions

We have shown that the block copolymer molecular architecture significantly influenced the self-assembly behavior of supramolecular comb−coil complexes. In this study, we investigated the microphase separation behavior of a $(PS)_5(P2VP)_5$ heteroarm star copolymer complexed with DBSA and compared the results with those reported previously for the linear PS-*b*-P2VP(DBSA) and the block-arm $(PS\text{-}b\text{-}P2VP)_5(PS)_5$(DBSA) complex. Despite the complex molecular architecture, the $(PS)_5(P2VP)_5$(DBSA) comb−coil complex exhibited hierarchical structure similar to that observed for the linear complex. However, the junction constraint, resulting from grouping several dissimilar chains to a common junction point, significantly influenced the ordered-state morphology and ODT of $(PS)_5(P2VP)_5$ copolymer in both the neat and complex state. The neat $(PS)_5(P2VP)_5$ copolymer exhibited a higher T_{ODT} than neat PS-*b*-P2VP due to different strengths of composition fluctuation associated with the difference in molecular architecture. The T_{ODT} of the small-scale lamellar mesophase formed by the P2VP(DBSA) comb blocks in $(PS)_5(P2VP)_5$(DBSA) complex was significantly higher than that observed for the linear complex. This was attributed to the lower entropy of transition in the heteroarm complex due to the junction constraint. The interdomain spacing of the larger-scale copolymer domains in the $(PS)_5(P2VP)_5$(DBSA) complex was smaller than that observed in the linear complex due to lower association number of the PS cylindrical microdomains because of chain crowding at the interface. However, the interdomain spacing was significantly larger compared to that in the block-arm complex due to different molecular segregation mechanism in the two star copolymers. We would like to note that although a slight polydispersity in arm number was inevitably present in the heteroarm copolymer used in this study, our conclusions were not influenced by this effect because the peculiar behavior associated with the ODT and the interdomain distance revealed here was governed by the junction constraint imposed by the star architecture of the copolymer under study. Hence, the conclusions drawn here held as long as the heteroarm architecture was present.

Acknowledgment. We gratefully acknowledge financial support from the National Science Council under Contract NSC 94-2216-E-007-039.

Supporting Information Available: Temperature-dependent POM micrographs, TEM micrograph, synchrotron SAXS profile of LA(DBSA) complex, and GPC characterization of the polymer synthesized. This material is available free of charge via the Internet at http://pubs.acs.org.

References and Notes

(1) Leibler, L. *Macromolecules* **1980**, *13*, 1602.
(2) Bates, F. S.; Fredrickson, G. H. *Annu. Rev. Phys. Chem.* **1990**, *41*, 525.
(3) Chen, J. T.; Thomas, E. L.; Ober, C. K.; Mao, G.-P. *Science* **1996**, *273*, 343.
(4) Hamley, I. W. *The Physics of Block Copolymers*; Oxford University Press: New York, 1998.
(5) Bates, F. S.; Fredrickson, G. H. *Phys. Today* **1999**, *52*, 32.
(6) Lodge, T. P. *Macromol. Chem. Phys.* **2003**, *204*, 265.
(7) Hadjichristidis, N.; Pispas, S.; Floudas, G. *Block Copolymers: Synthetic Strategies, Physical Properties, and Applications*; Wiley-Interscience: New York, 2003.
(8) Plate', N. A.; Shibaev, V. P. *Comb-Shaped Polymers and Liquid Crystals*; Plenum Press: New York, 1987.
(9) Antonietti, M.; Conrad, J.; Thünemann, A. *Macromolecules* **1994**, *27*, 6007.
(10) Ikkala, O.; Ruokolainen, J.; ten Brinke, G.; Torkkeli, M.; Serimaa, R. *Macromolecules* **1995**, *28*, 7088.
(11) Ruokolainen, J.; ten Brinke, G.; Ikkala, O.; Torkkeli, M.; Serimaa, R. *Macromolecules* **1996**, *29*, 3409.
(12) ten Brinke, G.; Ikkala, O. *Trends Polym. Sci.* **1997**, *5*, 213.
(13) Ruokolainen, J.; Mäkinen, R.; Torkkeli, M.; Mäkelä, T.; Serimaa, R.; ten Brinke, G.; Ikkala, O. *Science* **1998**, *280*, 557.
(14) Ikkala, O.; Knaapila, M.; Ruokolainen, J.; Torkkeli, M.; Serimaa, R.; Jokela, K.; Horsburgh, L.; Monkman, A.; ten Brinke, G. *Adv. Mater.* **1999**, *11*, 1206.
(15) Chen, H. L.; Hsiao, M. S. *Macromolecules* **1999**, *32*, 2967.
(16) Ruokolainen, J.; Eerikainen, H.; Torkkeli, M.; Serimaa, R.; Jussila, M.; Ikkala, O. *Macromolecules* **2000**, *33*, 9272.
(17) Hartikainen, J.; Lahtinen, M.; Torkkeli, M.; Serimaa, R.; Valkonen, J.; Rissanen, K.; Ikkala, O. *Macromolecules* **2001**, *34*, 7789.
(18) Kato, T.; Mizoshita, N.; Kanei, K. *Macrol. Rapid Commun.* **2001**, *22*, 797.
(19) Ikkala, O.; ten Brinke, G. *Science* **2002**, *295*, 2407.

(20) Chen, H. L.; Ko, C. C.; Lin, T. L. *Langmuir* **2002**, *18*, 5619.
(21) Nandan, B.; Chen, H. L.; Liao, C. S.; Chen, S. A. *Macromolecules* **2004**, *37*, 9561.
(22) Ruokolainen, J.; Saariaho, M.; Ikkala, O.; ten Brinke, G.; Thomas, E. L.; Torkkeli, M.; Serimaa, R. *Macromolecules* **1999**, *32*, 1152.
(23) Ruokolainen, J.; ten Brinke, G.; Ikkala, O. *Adv. Mater.* **1999**, *11*, 777.
(24) Ruotsalainen, T.; Torkkeli, M.; Serimaa, R.; Mäkelä, T.; Mäki-Ontto, R.; Ruokolainen, J.; ten Brinke, G.; Ikkala, O. *Macromolecules* **2003**, *36*, 9437.
(25) Polushkin, E.; Alberda van Ekenstein, G.; Dolbnya, I.; Bras, W.; Ikkala, O.; ten Brinke, G. *Macromolecules* **2003**, *36*, 1421.
(26) Alberda van Ekenstein, G.; Polushkin, E.; Nijland, H.; Ikkala, O.; ten Brinke, G. *Macromolecules* **2003**, *36*, 3684.
(27) Valkama, S.; Ruotsalainen, T.; Kosonen, H.; Ruokolainen, J.; Torkkeli, M.; Serimaa, R.; ten Brinke, G.; Ikkala, O. *Macromolecules* **2003**, *36*, 3986.
(28) Kosonen, H.; Valkama, S.; Ruokolainen, J.; Torkkeli, M.; Serimaa, R.; ten Brinke, G.; Ikkala, O. *Eur. Phys. J. E* **2003**, *10*, 69.
(29) Valkama, S.; Kosonen, H.; Ruokolainen, J.; Haatainen, T.; Torkkeli, M.; Serimaa, R.; ten Brinke, G.; Ikkala, O. *Nat. Mater.* **2004**, *3*, 872.
(30) Ikkala, O.; ten Brinke, G. *Chem. Commun.* **2004**, *19*, 2131.
(31) Bondzic, S.; de Wit, J.; Polushkin, E.; Schouten, A. J.; ten Brinke, G.; Ruokolainen, J.; Ikkala, O.; Dolbnya, I.; Bras, W. *Macromolecules* **2004**, *37*, 9517.
(32) Tsao, C.-S.; Chen, H.-L. *Macromolecules* **2004**, *37*, 8984.
(33) ten Brinke, G.; Ikkala, O. *Chem. Rec.* **2004**, *4*, 219.
(34) Polushkin, E.; Bondzic, S.; de Wit, J.; Alberda van Ekenstein, G.; Dolbnya, I.; Bras, W.; Ikkala, O.; ten Brinke, G. *Macromolecules* **2005**, *38*, 1804.
(35) Nandan, B.; Lee, C.-H.; Chen, H.-L.; Chen, W.-C. *Macromolecules* **2005**, *38*, 10117.
(36) Olvera de la Cruz, M.; Sanchez, I. C. *Macromolecules* **1986**, *19*, 2501.
(37) Dobrynin, A. V.; Erukhimovich, I. Ya. *Macromolecules* **1993**, *26*, 276.
(38) Milner, S. T. *Macromolecules* **1994**, *27*, 2333.
(39) Olmsted, P. D.; Milner, S. T. *Macromolecules* **1998**, *31*, 4011.
(40) Floudas, G.; Hadjichristidis, N.; Iatrou, H.; Pakula, T.; Fischer, E. W. *Macromolecules* **1994**, *27*, 7735.
(41) Floudas, G.; Pispas, S.; Hadjichristidis, N.; Pakula, T.; Erukhimovich, I. *Macromolecules* **1996**, *29*, 4142.
(42) Floudas, G.; Paraskeva, S.; Hadjichristidis, N.; Fytas, G.; Chu, B.; Semenov, A. N. *J. Chem. Phys.* **1997**, *107*, 5502.
(43) Floudas, G.; Hadjichristidis, N.; Iatrou, H.; Avgeropoulos, A.; Pakula, T. *Macromolecules* **1998**, *31*, 6943.
(44) Buzza, D. M. A.; Hamley, I. W.; Fzea, A. H.; Moniruzzaman, M.; Allgaier, J. B.; Young, R. N.; Olmsted, P. D.; McLeish, T. C. B. *Macromolecules* **1999**, *32*, 7483.
(45) Ishizu, K.; Uchida, S. *Prog. Polym. Sci.* **1999**, *24*, 1439.
(46) Beyer, F. L.; Gido, S. P.; Uhrig, D.; Mays, J. W.; Tan, N. B.; Trevino, S. F. *J. Polym. Sci., Polym. Phys.* **1999**, *37*, 3392.
(47) Beyer, F. L.; Gido, S. P.; Velis, G.; Hadjichristidis, N.; Tan, N. B. *Macromolecules* **1999**, *32*, 6604.
(48) Grayer, V.; Dormidontova, E. E.; Hadziioannou, G.; Tsitsilianis, C. *Macromolecules* **2000**, *33*, 6330.
(49) Matsen, M. W.; Gardiner, J. M. *J. Chem. Phys.* **2000**, *113*, 1673.
(50) Zhu, Y.; Gido, S. P.; Moshakou, M.; Iatrou, H.; Hadjichristidis, N.; Park, S.; Chang, T. *Macromolecules* **2003**, *36*, 5719.
(51) Tsitsilianis, C.; Voulgaris, D. *Macromol. Chem. Phys.* **1997**, *198*, 997 and references therein.
(52) Park, S.; Cho, D.; Im, K.; Chang, T.; Uhrig, D.; Mays, J. W. *Macromolecules* **2003**, *36*, 5834.
(53) de Gennes, P. G. *Scaling Concepts in Polymer Physics*; Cornell University Press: Ithaca, NY, 1985.
(54) Dobrynin, A. V.; Erukhimovich, I. Y. *J. Phys. II* **1991**, *1*, 1387.
(55) Sakamoto, N.; Hashimoto, T. *Macromolecules* **1998**, *31*, 8493.
(56) Sakamoto, N.; Hashimoto, T.; Han, C. D.; Kim, D.; Vaidya, N. Y. *Macromolecules* **1997**, *30*, 1621.
(57) Han, C. D.; Vaidya, N. Y.; Kim, D.; Shin, G.; Yamaguchi, D.; Hashimoto, T. *Macromolecules* **2000**, *33*, 3767.
(58) Vaidya, N. Y.; Han, C. D.; Kim, D.; Sakamoto, N.; Hashimoto, T. *Macromolecules* **2001**, *34*, 222.
(59) Kim, J. K.; Lee, H. H.; Sakurai, S.; Aida, S.; Masamoto, J.; Nomura, S.; Kitagawa, Y.; Suda, Y. *Macromolecules* **1999**, *32*, 6707.
(60) Sakamoto, N.; Hashimoto, T.; Han, C. D.; Kim, D.; Vaidya, N. Y. *Macromolecules* **1997**, *30*, 5321.
(61) Pispas, S.; Poulos, Y.; Hadjichristidis, N. *Macromolecules* **1998**, *31*, 4177.
(62) Voulgaris, D.; Tsitsilianis, C.; Grayer, V.; Esselink, F. J.; Hadziioannou, G. *Polymer* **1999**, *40*, 5879.
(63) Chang, Y.; Chen, W.-C.; Sheng, Y.-J, Jiang, S.; Tsao, H.-K. *Macromolecules* **2005**, *38*, 6201.

MA060042T